1

Measurements of the photon detection efficiency done for Geiger-mode avalanche photodiodes (G-APD)

S. Gentile and F. Meddi

Università degli Studi di Roma "La Sapienza",
Piazzale Aldo Moro 5, 00185 Roma, Italy

E. Kuznetsova

DESY,
Notkestraße 85, 22607, Hamburg, Germany
E-mail: kkuzn@ifh.de

Estimation of the Photon Detect Efficiency (PDE) of multi-pixel Geiger-mode avalanche photodiodes (G-APD) based on measurements of the G-APD response to low-intensity light is presented. The fit of the light-response spectra takes into account after-pulsing and cross-talk effects and yields the value of initial photons. Using a calibrated photo-detector as a reference, the value of the PDE can be calculated. The sources of systematic error of the obtained PDE is discussed as well as possibility for its minimization.

Keywords: G-APD; SiPM; PDE; cross-talk; after-pulsing .

1. Introduction

Multi-pixel Geiger-mode avalanche photodiodes (G-APDs) is a solid-state photodetector based on a rapidly developing technology.[1–6] Having characteristics comparable to the ones of vacuum photomultipliers and being unsensitive to magnetic field, the G-APDs are widely considered as attractive photo-detectors for High-Energy[7,8] and Neutrino Physics[9] experiments.

Measurements of the G-APD response to low-intensity light is a standard procedure done to determine voltage corresponding to a desired gain. An accurate fit of the response spectra yields also after-pulsing and cross-talk contributions. The measurements done with a calibrated reference detector allow to estimate the PDE of the G-APD from the response spectra as well.

2

2. Measurement Set-Up

Fig. 1 (left) shows a general scheme of the PDE measurements. The light from a light-emitting diode (LED) operated in a pulse-mode is delivered to an optical filter. The optical filters used for the measurements corresponded to the wavelength of the LED and have FWHM of $3 - 10$ nm. The filtered light was routed to a light-tight thermostabilized box with two photo-detectors. As a reference detector a PMT-based photosensor module H5783P produced and calibrated by HAMAMATSU was used. Both PMT and G-APD have the effective areas (Ø8 mm and 1×1 mm^2 correspondingly) much larger than 50 μm of the fiber core diameter. The reference photosensor module has an FC type fiber adapter providing a reliable optical coupling between the fiber and PMT window with the distance less than 5 mm. A G-APD was fixed on an xyz-table, the distance between the fiber edge and effective area was set to be about 5 mm.

The fiber between the optical filter and the light-tight box was reconnected for the measurements with a particular photodetector at the box side. To estimate and correct for the systematic error caused by the reconnections and different optical couplings from the box connectors to the photodetectors, additional measurements were performed when the individual PMT and G-APD fibers where cross-connected.

Fig. 1 (right) shows the read-out scheme of the G-APD. The signal from G-APD is read out with a charge-sensitive preamplifier and digitized with an integrating ADC. The LED pulse of about 6 ns duration and ADC gate of about 65 ns width was synchronized by means of a common trigger. In case of the reference photosensor the direct signal from PMT was amplified with an external amplifier and digitized with the ADC.

The results discussed here are obtained for HAMAMATSU produced Multi-Pixel Photon Counter S10362-11-025C[10] operated at the gain of $\sim 2.75 \times 10^5$.
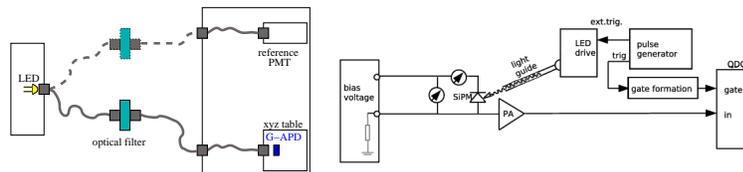

Fig. 1.   General scheme of the PDE measurements (left) and G-APD read-out (right).

3. Measurement results and fit procedure

Reference PMT: The measurements were done for a low number of photons and the response of the reference PMT can be well described as a convolution of the Poisson and Gauss distributions.

$$N(x) = N \times \sum_n \left(\mathrm{Gauss(x, \mu_n, \sigma_n)} \times \mathrm{Poisson(n, \lambda)} \right), \tag{1}$$

where x is the charge in ADC counts, n is the number of photons detected, λ is the mean number of the detected photons, $\mu_n = \mu_0 + n \times \mathrm{gain}$ - charge in ADC counts corresponding to n photons detected, $\sigma_n^2 = \sigma_0^2 + n \times \sigma_1^2$ - width of the signal from n detected photons as a superposition of the electronic noise (σ_0) and the signal fluctuation (σ_1).

Due to additional electrical noise caused by the external amplifier, the pedestal peak had non-gaussian shape. However, this shape is well described as superposition of three gaussian peaks, two of which are considered to be symmetric. Fig. 2 (left) shows the pedestal fitted to the sum of three gaussians. Fig. 2 (right) shows the signal spectrum fitted according to Eq. 1 with the correction for the triple-gaussian noise.

Using the mean number of photons obtained from the above fit and the PMT efficiency table provided by HAMAMATSU for the used photosensor module, the mean number of photons delivered by the optical system to a surface of a photodetector per an LED pulse was estimated.
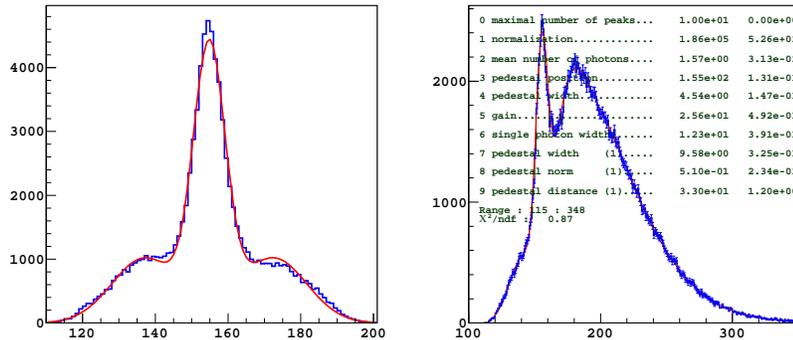

Fig. 2.   The pedestal (left) and signal (right) spectra obtained with the reference PMT.

4

G-APD: Fig. 3 shows the noise (left) and signal (right) spectra obtained with the G-APD. The noise spectrum shows relatively low contribution of signals caused by the thermogeneration. Estimated as a ratio of the number of events contributing to non-pedestal peaks to the total number of events, this contribution gives about 2%. This allows to neglect the thermogeneration probability in the fit of the signal spectrum.

However, a ratio of the numbers of events contributing to the second non-pedestal peak and to the first one gives the rough estimation of the cross-talk value to be about 20% and requires to take the cross-talk effect into account.

Additional peaks seen in the signal spectrum between the peaks corresponding to i and $(i + 1)$ fired cells were considered to be caused by after-pulsing.[11] To observe the neseccary correction function describing the after-pulsing (AP) contribution to the signal spectrum, the main peaks fitted to an ideal gaussian shape were subtracted from the spectrum. The resulting distribution is shown in Fig. 4 (left). As it is seen, for this G-APD and for the chosen gate length the AP contribution to an ith peak can be well described as a sum of two gaussians.

An event without AP contributes to the ideal gaussian peak corresponding to i fired cells and occurs with probability $P_i^{\text{noAP}} = P_i^0 \times (1 - P_{\text{AP}})^i$, where P_i^0 is probability to get initially i cells fired and P_{AP} is a probability to get an AP from one cell. Correspondingly, the probability to have any number of AP contributing to the ith peak is $P_i^{\text{AP}} = 1 - P_i^{\text{noAP}} =$
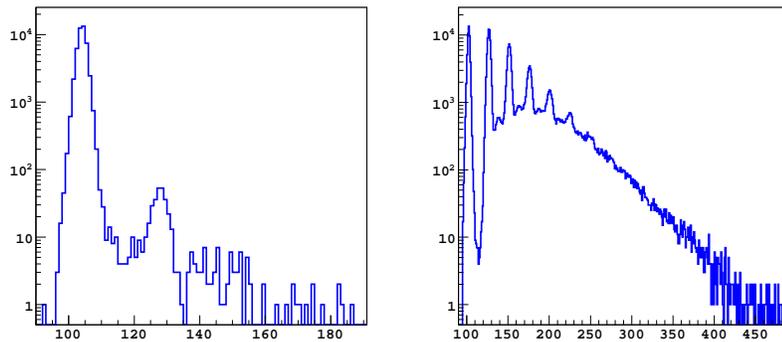

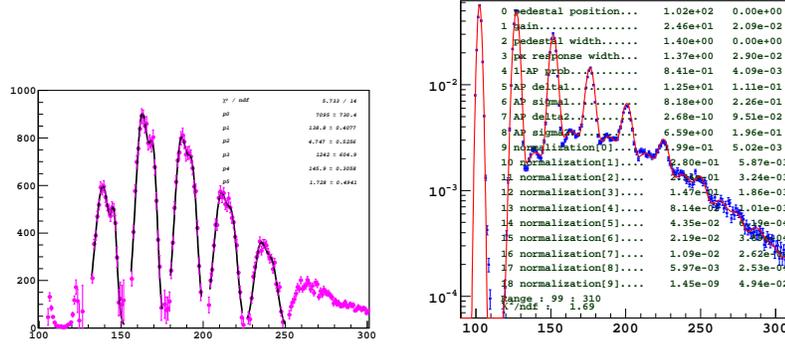Fig. 3.   The pedestal (left) and signal (right) spectra obtained with the HAMAMATSU G-APD.

Fig. 4.   Residual distribution after a subtraction of best-fitted ideal gaussians from the signal spectrum (left).

$P_i^0 \times (1-(1-P_{\mathrm{AP}})^i)$. The double-peak structure of the AP was considered to be caused by second-order effects and, assuming the same probability P_{AP}, the resulting signal shape was described as $P(x) = P_i^{\mathrm{noAP}} \times G(\mu_i, \sigma_i) + P_i^{\mathrm{AP1}} \times G(\mu_i + \delta_1, \sigma_1) + P_i^{\mathrm{AP2}} \times G(\mu_i + \delta_2, \sigma_2)$,, where μ_i and σ_i are calculated the same way as for Eq. 1. Here $P_i^{\mathrm{AP1}} = P_i^0 \times (1-(1-P_{\mathrm{AP}})^i) \times (1-P_{\mathrm{AP}})^j$, $P_i^{\mathrm{AP2}} = P_i^0 \times (1-(1-P_{\mathrm{AP}})^i) \times (1-(1-P_{\mathrm{AP}})^j)$ and $0 < j < i$. The result of the fit done with P_i^0 taken as free parameters is shown in Fig. 4 (right). P_{AP} is obtained to be at the level of 15%.

In an ideal case without cross-talk the values of P_i^0 are distributed according to the Poisson statistics. If cross-talk probability $\varepsilon \neq 0$, then the first non-pedestal peak is contributed from one initially fired cell without cross-talk with probability $P_1^0(1-\varepsilon)$. The second peak corresponds to two initially fired cells without cross-talk and one fired cell caused a cross-talk: $P_2^0(1-\varepsilon)^2 + P_1^0\varepsilon(1-\varepsilon)$. The resulting probability to observe i fired cell is $\sum_{j=0}^{i} P_j^0(1-\varepsilon)^j\varepsilon^{i-j}B(i-1, j-1)$, where $B(i-1, j-1)$ are binomial coefficients. Fig. 5 (left) shows the the probabilities to observe i fired cells P_i^0 obtained from the signal fit and fitted to the above distribution. The obtained value for the cross-talk probability ε is at the level of 20%. The mean number of initial photons derived from the fit was used to calculate PDE.
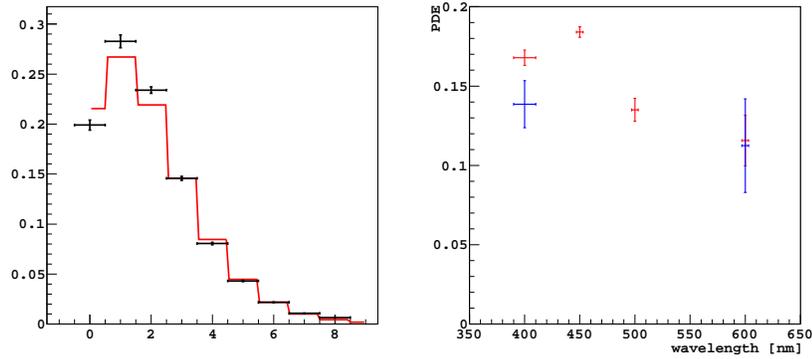
6

Fig. 5.   The fit of the probabilities to observe i fired cells P_i^0 obtained from the signal fit (left) and the calculated PDE as a function of the light wavelength.

4. Conclusion

Fig. 5 (right) shows the preliminary results from the PDE calculation based on the above fitting procedure. The measurements done with the direct (red) and cross connection (blue) of the optical fibers are shown. The difference obtained for this two kind of measurements represents the systematic error caused by the measurement and fit procedure.

The improvement of the fit procedure and systematic analysis of the measurements with the cross connections will allow to reduce the systematics.

References

1. G. Bondarenko *et al.*, *Nucl. Phys. Proc. Suppl.* **61B**, 347 (1998).
2. P. Buzhan *et al.*, *Nucl. Instrum. Meth.* **A504**, 48 (2003).
3. V. Golovin and V. Saveliev, *Nucl. Instrum. Meth.* **A518**, 560 (2004).
4. B. Dolgoshein *et al.*, *Nucl. Instrum. Meth.* **A563**, 368 (2006).
5. K. Yamamoto *et al.*, *IEEE Nucl. Sci. Symp. Conf. Rec.* **2**, 1094 (2006).
6. N. Dinu *et al.*, *Nucl. Instrum. Meth.* **A572**, 422 (2007).
7. M. Danilov, *Nucl. Instrum. Meth.* **A581**, 451 (2007).
8. J. R. A. Heering *et al.*, *Nucl. Instrum. Meth.* **A576**, p. 341349 (2007).
9. M. Yokoyama *et al.*, *Nucl. Instrum. Meth.* **A, In Press**.
10. HAMAMATSU PHOTONICS K.K, Product catalogue No. KAPD0002E02 (2007).
11. G. Pauletta *et al.*, *PoS* **(PD07)014** (2007).